Active control of vortex-induced vibrations of a circular cylinder using windward-suction- leeward-blowing actuation

Chenglei Wang, Hui Tang (iD), Simon C. M. Yu, and Fei Duan

View Online **Export Citation** **CrossMark**

ARTICLES YOU MAY BE INTERESTED IN

Active control of vortex-induced vibrations of a circular cylinder using windward-suction-leeward-blowing actuation

Chenglei Wang,[1,2] Hui Tang,[2,a)] Simon C. M. Yu,[3] and Fei Duan[1]

[1]*School of Mechanical and Aerospace Engineering, Nanyang Technological University, Singapore 639798, Republic of Singapore*
[2]*Department of Mechanical Engineering, The Hong Kong Polytechnic University, Kowloon, Hong Kong, China*
[3]*Singapore Institute of Technology, Singapore 179104, Republic of Singapore*

This paper studies the control of two-dimensional vortex-induced vibrations (VIVs) of a single circular cylinder at a Reynolds number of 100 using a novel windward-suction-leeward-blowing (WSLB) concept. A lattice Boltzmann method based numerical framework is adopted for this study. Both open-loop and closed-loop controls are implemented. In the open-loop control, three types of actuation arrangements, including the pure suction on the windward side of the cylinder, the pure blowing on the leeward side, and the general WSLB on both sides, are implemented and compared. It is found that the general WSLB is the most effective, whereas the pure suction is the least effective. In the closed-loop control, the proportional (P), integral (I), and proportional-integral (PI) control schemes are applied to adjust the WSLB velocities according to the flow information obtained from a sensor. The effects of four key control parameters including the proportional gain constant, the integral gain constant, the length of data history used for the feedback, and the location of the sensor are investigated. It is found that the use of only P control fails to completely suppress the VIV, the use of only I control can achieve the complete suppression, and the PI control performs the best in terms of both the control effectiveness and efficiency. In the PI control, there exists an optimal length of data history for the feedback, at which the VIV control is the most efficient. There also exist the minimum required WSLB velocities for the VIV suppression, independent of the control schemes. Moreover, it is found that the VIV control is independent of the sensor location. *Published by AIP Publishing.* [http://dx.doi.org/10.1063/1.4947246]

I. INTRODUCTION

Flow past a bluff body can cause asymmetric vortex shedding when the Reynolds number exceeds a critical value, resulting in dynamic loading on the bluff body. If the bluff body is allowed to move, vortex induced vibrations (VIVs) occur. Once the vortex shedding frequency matches the body structure's natural frequency, large-amplitude vibration happens, which may cause catastrophic failures to the structure. Since various structures that are immersed in flows, such as airplanes, automobiles, and offshore structures, have been widely applied in engineering practice, it is desired to explore effective and efficient VIV control methods to attenuate the asymmetric vortex shedding and mitigate the resulting VIVs, so as to prevent the associated structures from being damaged.

Various VIV control methods are available, which can generally be classified into two major categories: passive (no power input required) and active (power input required).[1] Passive VIV control is usually achieved through modifying the geometry of a bluff body. It does not require energy input and hence is easy to implement. As such, it has been extensively used in various VIV

---

a)h.tang@polyu.edu.hk

controls.[1–5] However, passive VIV control methods do not have the ability to provide on-demand control, and usually they are only effective in a narrow operational range. By injecting a small and tunable amount of energy into the ambient flow, active VIV control methods can perform more adaptively and effectively. Numerous active methods have been applied to manipulate the asymmetric wakes behind bluff bodies so as to attenuate the resulting VIVs, such as the moving surface boundary-layer control,[6] plasma jets,[7] flush-mounted piezoelectric actuators,[8] synthetic jets,[9] pure suction,[10] pure blowing,[11] rotational oscillation,[12] traveling wave wall,[13] and electromagnetic method.[14] Recently, a novel flow control means, i.e., the windward-suction-leeward-blowing (WSLB) concept, was proposed by Dong *et al.*[15] for the VIV control. In this concept, the actuator consists of a pair of suction slots at the windward side of the bluff body and a pair of blowing slots at the leeward side. If the suction velocity matches the blowing velocity, the WSLB actuator works as a zero net mass flux actuator, but produces non-zero momentum flux. In this case, it does not require complex piping systems for mass delivery, making its implementation relatively easy.

Most of the past studies on active VIV control only focused on controlling the cross-flow VIVs, i.e., one-dimensional VIVs. Two-dimensional (cross-flow and streamwise) VIVs, which are more common in the real-world applications, was actively controlled in only a few studies.[13,16] By using the WSLB, Dong *et al.*[15] controlled the one-dimensional VIV of a circular cylinder and found that the wake instability was modified, which resulted in the attenuation of the lift fluctuations as well as the cross-flow VIVs.

In this study, we extend the application of the WSLB concept to the control of two-dimensional VIVs of a circular cylinder. The diameter-based Reynolds number is fixed at 100, at which the flow is intrinsically two-dimensional.[17] To facilitate this study, a lattice Boltzmann method (LBM) based numerical framework is adopted. Both the open-loop (i.e., control input is independent of the flow state) and the closed-loop (i.e., control input varies with the flow state) control schemes are implemented. Although various advanced closed-loop control schemes have been used for VIV control, such as the adaptive fuzzy sliding mode scheme[16] and the adaptive least-mean-square scheme,[18] three basic schemes are used in the present study, including the proportional (P), integral (I), and proportional-integral (PI) control schemes. The performances of the WSLB in two-dimensional VIV control under these control schemes are examined and compared.

II. PROBLEM DESCRIPTION AND METHODOLOGY

A. Problem description

As shown in Figure 1, a circular cylinder immersed in a uniform flow at a diameter-based Reynolds number $Re = 100$ is connected with two identical springs, one in the x (streamwise) direction and the other in the y (cross-flow) direction, so that it can move in the two-dimensional space. The dynamics of this cylinder is governed by

$$m\ddot{x} + Kx = F_D,$$ (1)

$$m\ddot{y} + Ky = F_L,$$ (2)

where m is the mass of the cylinder, K the spring stiffness, F_D and F_L the drag and lift forces experienced by the cylinder, respectively. Nondimensionalizing these two governing equations gives

$$\frac{\mathrm{d}^2 x^*}{\mathrm{d}t_r^{*2}} + \left(\frac{4\pi^2}{U_R^2}\right)x^* = \frac{C_D}{2m^*},$$ (3)

$$\frac{\mathrm{d}^2 y^*}{\mathrm{d}t_r^{*2}} + \left(\frac{4\pi^2}{U_R^2}\right)y^* = \frac{C_L}{2m^*},$$ (4)

where $x^* = x/D$, $y^* = y/D$, $t_r^* = U_\infty t/D$, D is the cylinder diameter, and U_∞ is the freestream velocity. m^* is the mass ratio defined as
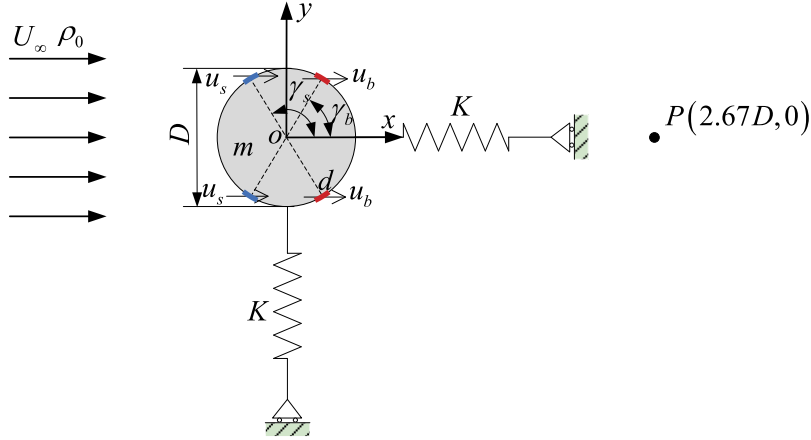
$$m^* = \frac{m}{\rho_0 D^2},$$ (5)

FIG. 1. Schematic of a two-dimensional vibrating circular cylinder equipped with the WSLB actuator in a uniform flow. U_∞ is the freestream velocity, D the cylinder diameter, and K the stiffness of the two springs. The two short blue line sections represent the two suction slots at the windward side of the cylinder, and the two short red line sections represent the two blowing slots at the leeward side. Point P located at $(2.67D, 0)$ is a sensor for the feedback control.

where ρ_0 is the fluid density. U_R is the reduced velocity defined as

$$U_R = \frac{U_\infty}{f_N D},\tag{6}$$

where f_N is the natural frequency of the present mass-spring system in vacuum in either the streamwise or the cross-flow direction

$$f_N = \frac{1}{2\pi}\sqrt{\frac{K}{m}}.\tag{7}$$

C_D and C_L are the drag and lift coefficients, respectively, defined as

$$C_D = \frac{2F_D}{\rho_0 U_\infty^2 D},\tag{8}$$

$$C_L = \frac{2F_L}{\rho_0 U_\infty^2 D}.\tag{9}$$

Note that in the present study m^* and U_R are fixed at 2 and 5, respectively, to ensure relatively large vibrations of the cylinder, which however are difficult to suppress.[12]

To control the cylinder's two-dimensional VIVs, a WSLB actuator is implemented on the surface of the cylinder as shown in Figure 1. The actuator consists of a pair of suction slots at the windward side of the cylinder (slot width $d = \pi D/72$, position angle $\gamma_s = 110°$) and a pair of blowing slots at the leeward side (slot width $d = \pi D/72$, position angle $\gamma_b = 70°$). The suction and blowing velocities relative to the moving cylinder are u_s and u_b, respectively, both in the streamwise direction.

In the present study, the capability of the WSLB operating with both open-loop and closed-loop control schemes in suppressing the cylinder's two-dimensional VIVs is investigated. In the open-loop control, two special cases, i.e., pure suction (i.e., $u_s \neq 0$ and $u_b = 0$) and pure blowing (i.e., $u_s = 0$ and $u_b \neq 0$), are also examined and compared with the general WSLB (i.e., $u_s = u_b \neq 0$) control. In the closed-loop control, however, only the general WSLB is investigated. To facilitate the closed-loop control, the P, I, and PI control schemes are applied, and the standard deviation of the y velocity, σ_v, at a randomly selected sensor location $P(2.67D, 0)$ (see Figure 1) over a certain period T_{SD} is chosen as the feedback signal. Since the target value for σ_v at the steady state is 0, σ_v itself represents the error between the actual value and the target value. As such, the relation between the velocities (u_s and u_b) and the feedback signal (σ_v) can be expressed as

$$u_s = u_b = K_p \sigma_v(t) + K_i \int_0^\tau \sigma_v(t)\,d\tau,\tag{10}$$

where K_p is the proportional gain constant and K_i is the integral gain constant. Note that, instead of the standard deviation of the x velocity or of the total velocity, the standard deviation of the y velocity σ_v is chosen as the feedback signal because it is the best choice for the present underactuated system. As will be revealed in Sec. III C 1, in some cases the use of the other two quantities as the feedback signal may result in the amplification, instead of suppression, of VIVs.

B. Methodology

To facilitate this study, the incompressible D2Q9 MRT LBE model,[19] i.e., two-dimensional incompressible multiple-relaxation-time lattice Boltzmann equation model with nine discrete velocities, is employed to simulate the two-dimensional flow around the circular cylinder. The MRT multi-block scheme proposed by Yu[20] is applied to enhance computational efficiency while maintaining sound accuracy. Besides, the overlap mesh combined with the interpolated half-way bounce back scheme[21] is incorporated to deal with moving curved boundaries and the corrected momentum exchange method[22] is employed for accurate prediction of the aerodynamic forces on the cylinder. To evaluate the capability of the WSLB in altering vortices in the cylinder wakes, the λ_{ci} criterion proposed by Zhou *et al.*[23] is employed to identify vortices. In this study, the isolines of $\lambda_{ci} = 0.2$ are used to define the vortex boundaries.

As shown in Figure 2, the computational domain is set as $60D(L) \times 20D(W)$ with a uniform flow coming from the left with a speed U_∞. The circular cylinder is initially placed at the centerline of the channel and $20D$ downstream from the inlet. The entire computational domain is divided into four sets of blocks with the mesh density being increased by a factor of 2 as the block number increases. That is, the block around the cylinder (i.e., Block 4) has the finest mesh with the lattice spacing $\triangle x = D/60$. The velocity of the uniform incoming flow is set as $U_\infty/c = 0.01$, where c is the lattice velocity. As such, the non-dimensional time step becomes $U_\infty \Delta t/D = 1/6000$.

The boundary conditions are also shown in Figure 2. At the inlet, the non-reflecting inlet boundary condition proposed by Izquierdo and Fueyo[24] is used, whereas at the outlet, the homogenous Neumann boundary condition is implemented. The Dirichlet boundary condition is applied at both the top and bottom walls, with an x velocity U_∞ and a y velocity 0. The WSLB actuator is represented by a number of nodes on the cylinder, and its time-dependent velocities are realized by enforcing u_s and u_b on these nodes. Details of the current numerical method and its validation can be found in our previous work.[9]

III. RESULTS AND DISCUSSIONS

A. Uncontrolled case

Figure 3 shows an instantaneous wake of the cylinder in the uncontrolled case, in which the normalized vorticity contour is presented and the identified vortices are enclosed by solid (positive
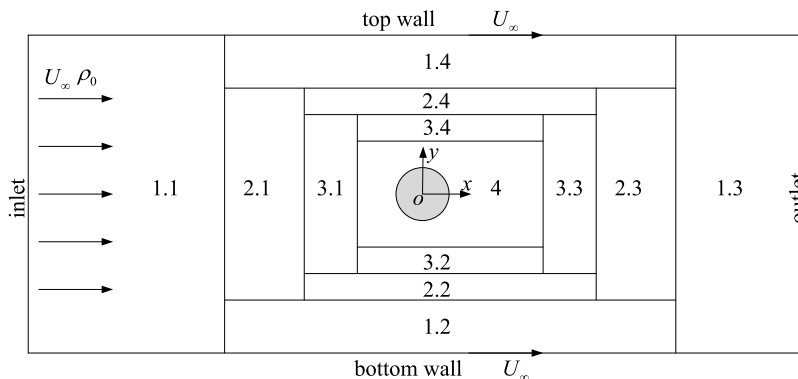

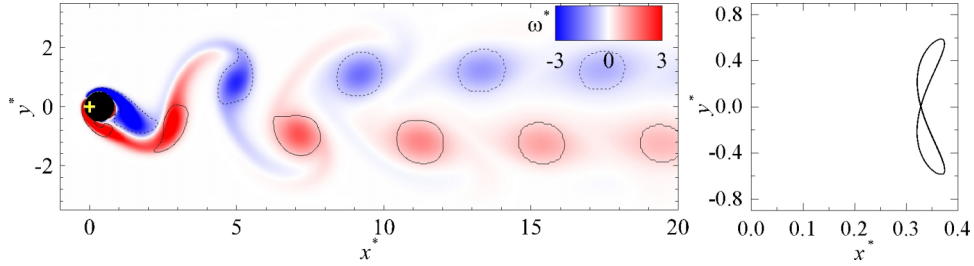FIG. 2. Computational domain with multi-block arrangement (not in scale).

FIG. 3. Wake pattern and cylinder trajectory of the uncontrolled case. The contour is the normalized vorticity $\omega^* = \omega D/U_\infty$, where ω is vorticity. The solid and dash lines represent vortices identified by $\lambda_{ci} = 0.2$ isolines enclosing positive and negative vorticities, respectively.

vortices) or dash (negative vortices) λ_{ci} isolines. The periodical vortex shedding stems from the interaction between the upper and lower alternatively growing vortices, and the wake converges to the 2S mode.[25] The lift and drag forces experienced by the cylinder vary periodically with time. As a result, the cylinder vibrates in both the streamwise and cross-flow directions and the trajectory of the cylinder center forms a figure "8." The standard deviation of the x and y displacements of the cylinder is $\sigma_{x_o^*} = 0.019$ and $\sigma_{y_o^*} = 0.416$, respectively. $\sigma_{y_o^*}$ is more than twenty times larger than $\sigma_{x_o^*}$, indicating the dominance of the cross-flow vibration in the uncontrolled case.

Note that the wake pattern shown in Figure 3 is taken at the instant when the cylinder approaches its equilibrium position from the lower half portion of the channel after the periodic steady state of the flow is achieved. This instant almost coincides with the instant when the lift experienced by the cylinder reaches zero from positive values. Hereafter in this study, the operation of the actuator in all the controlled cases starts at this instant, and all the wake patterns are also presented at this instant.

B. Open-loop control

Without using any feedback control scheme, nine cases are simulated to investigate the VIV control effects of the pure suction ($u_b = 0$, $u_s = U_\infty, 2U_\infty$ or $3U_\infty$), the pure blowing ($u_b = U_\infty, 2U_\infty$ or $3U_\infty$, $u_s = 0$), as well as the WSLB ($u_b = u_s = U_\infty, 2U_\infty$ or $3U_\infty$). The performance of these three actuation arrangements is quantified by $\sigma_{x_o^*}$ and $\sigma_{y_o^*}$, the standard deviation of the cylinder's x and y displacements. As shown in Figure 4, $\sigma_{x_o^*}$ and $\sigma_{y_o^*}$ in all the actuation arrangements are significantly smaller than those in the uncontrolled case, indicating that these three actuation arrangements are all able to effectively attenuate the VIVs. In addition, for each actuation arrangement, the control effect improves with the increase of the actuation velocity, which is revealed by the monotonic decrease of both $\sigma_{x_o^*}$ and $\sigma_{y_o^*}$.
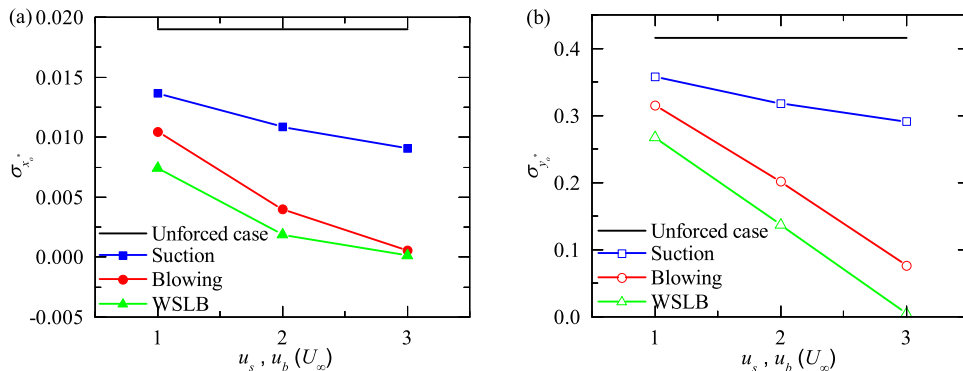

FIG. 4. Variation of $\sigma_{x_o^*}$ and $\sigma_{y_o^*}$, the standard deviation of the cylinder's x and y displacements, with u_s (or u_b) under the pure suction, pure blowing, and WSLB actuation with open-loop control.
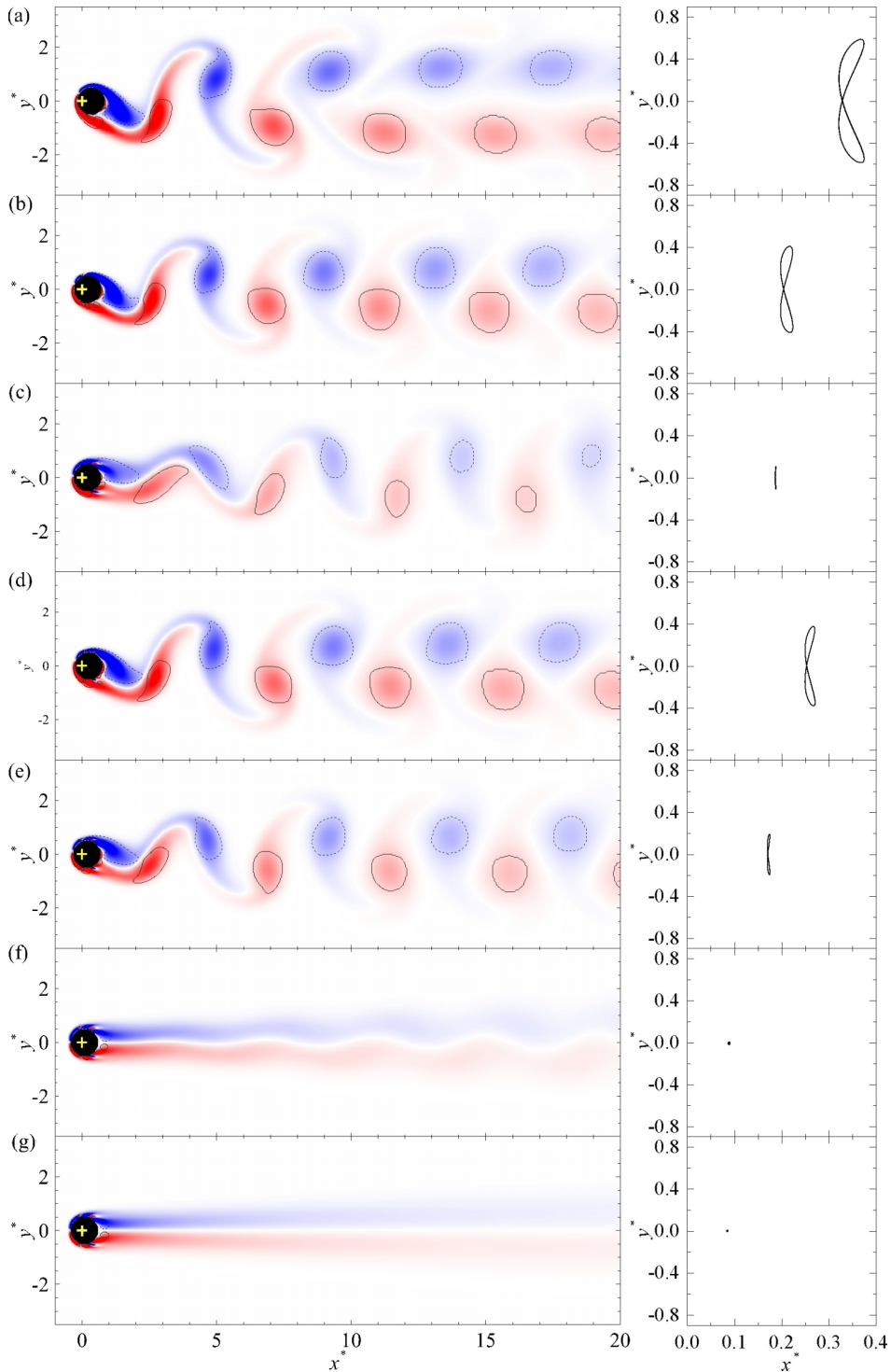
FIG. 5. Wake pattern and cylinder trajectory of (a) the uncontrolled case and the open-loop control cases with (b) $u_s = 3U_\infty$, $u_b = 0$; (c) $u_s = 0$, $u_b = 3U_\infty$; (d) $u_s = u_b = U_\infty$; (e) $u_s = u_b = 2U_\infty$; (f) $u_s = u_b = 3U_\infty$; (g) $u_s = u_b = 3.1U_\infty$. Refer to Figure 3 for the colorbar.

From Figure 4, it can also be seen that, with the same actuation velocity, the WSLB performs the best among the three actuation arrangements and the pure suction performs the worst. This is also confirmed by the cylinder's wakes and trajectories shown in Figures 5(b), 5(c) and 5(f), where the pure suction, pure blowing, and WSLB all operate with velocity $3U_\infty$. When the pure suction

is implemented (Figure 5(b)), although the cylinder's mean streamwise position is significantly pushed upstream due to the momentum introduced by the strong suction, its wake is not apparently altered compared to that in the uncontrolled case (Figure 5(a)), and the VIV is only slightly mitigated and still obvious. When the pure blowing is applied with the same strength (Figure 5(c)), however, the vortices in the wake become much smaller and weaker, and the VIV becomes much milder. In this case, the streamwise vibration of the cylinder is almost negligible but the cross-flow vibration is still observable. When the WSLB is applied (Figure 5(f)), the cylinder is further pushed upstream due to the doubling of the added momentum, the wake becomes more symmetric and no vortex is captured, and the VIV is almost fully suppressed.

The significant difference in the control effect between the pure suction and the pure blowing is mainly due to their different actuation locations. Since the pure suction is applied at the windward side of the cylinder, it does not directly interact with the wake. Instead, it affects the wake through changing the cylinder's motion. On the contrary, the pure blowing is applied at the leeward side of the cylinder. Hence it directly interacts with the developing shear layers and affects the resulting vortex shedding process, causing the significant change of the wake. Since the WSLB is the combination of the above two, it inherits the advantages of both control methods and hence performs the best.

The effect of the WSLB velocities is also studied. As shown in Figures 5(d)–5(g), with the velocity increasing from U_∞ to $3U_\infty$, the cylinder is pushed more and more upstream and the area enclosed by the trajectory becomes smaller and smaller. In addition, the identified vortices in the wake shrink and are closer to the channel centerline. When the WSLB velocities further increase to $3.1U_\infty$, the wake becomes perfectly symmetric and the VIV is completely suppressed, as shown in Figure 5(g). In this case, the cylinder is stationed at point $(0.085D, 0)$ after it achieves the steady state. Furthermore, it is found that $3.1U_\infty$ is the minimum WSLB velocities required to fully suppress the VIV in the open-loop control.

C. Closed-loop control

When the realtime flow information, i.e., the standard deviation of the y velocity σ_v at the sensor location P $(2.67D, 0)$, is fed back to the WSLB actuator, it is expected that the VIV control can be more effective and efficient. In this section, therefore, three basic closed-loop control schemes, i.e., the P, I, and PI control schemes, are applied, and their performance in suppressing the VIV is studied. Table I lists the selected cases, where T_{SD} is the length of data history used for the feedback and T_n is the vortex shedding period in the uncontrolled case. In the following, the performance of the three control schemes with $T_{SD} = T_n$ is discussed first, which is followed by the studies on the influences of T_{SD} and the sensor location.

1. P control

Figure 6 shows the variation of $\sigma_{x_o^*}$ and $\sigma_{y_o^*}$, i.e., the standard deviation of the x and y displacements of the vibrating cylinder, against the proportional gain constant K_p. It is seen that the variation trends for $\sigma_{x_o^*}$ and $\sigma_{y_o^*}$ are opposite. There exists a critical value 14 for K_p: when $K_p \leq 14$, $\sigma_{x_o^*}$ remains at small values, whereas it increases dramatically when $K_p > 14$, even greater than the value in the uncontrolled case. This implies that the use of small K_p can suppress the cylinder's streamwise vibration, whereas the use of large K_p amplifies the vibration. As for $\sigma_{y_o^*}$, it decreases

TABLE I. Selected P, I, and PI control cases.

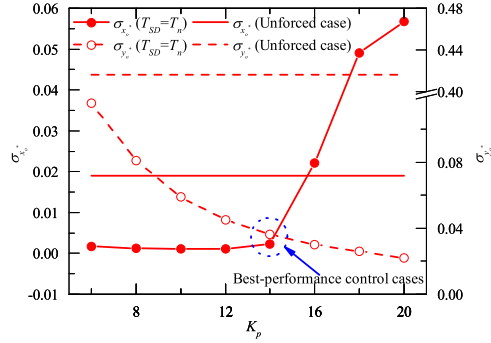| Cases	$T_{SD}(T_n)$	K_P	$K_i(\times 10^{-5})$
P control cases	1	6, 8, 10, 12, 14, 16, 18, 20	0
I control cases	1	0	2, 4, 6, 8
PI control cases	0, 1, 2, 4, 6, 8, 10	12	2, 4, 6, 8

FIG. 6. Variation of $\sigma_{x_o^*}$ and $\sigma_{y_o^*}$, the standard deviation of the cylinder's x and y displacements, with K_p for the P control cases.

monotonically with K_p, indicating that the larger K_p, the better suppression of the cylinder's cross-flow vibration. As such, a suitable K_p range exists for the control of the two-dimensional VIV, in which both streamwise and cross-flow vibrations are significantly attenuated. From Figure 6, it is found that the best control occurs at $K_p = 14$. However, note that in the selected cases $\sigma_{x_o^*}$ and $\sigma_{y_o^*}$ are all greater than zero, indicating that the use of only the P control scheme fails to completely suppress the VIV. This can also be confirmed in theory. Assuming $\sigma_v = 0$ at an instant, according to Equation (10) one can get $u_s = u_b = 0$, meaning that at this instant the cylinder is stationary and the WSLB is off. However, this status is not sustainable because the asymmetric vortex shedding will start naturally and the cylinder will experience the VIV again.

The wake patterns and the trajectories of three selected cases, i.e., $K_p = 6$, 12, and 18, are shown in Figure 7. At $K_p = 6$, the cylinder vibrates periodically with a much smaller and slimmer figure "8" compared to in the uncontrolled case. As K_p increases to 12, the cylinder still vibrates periodically but with even smaller amplitudes, and the size and strength of the vortices in the wake are significantly reduced. At $K_p = 18$, however, things become quite different. As shown
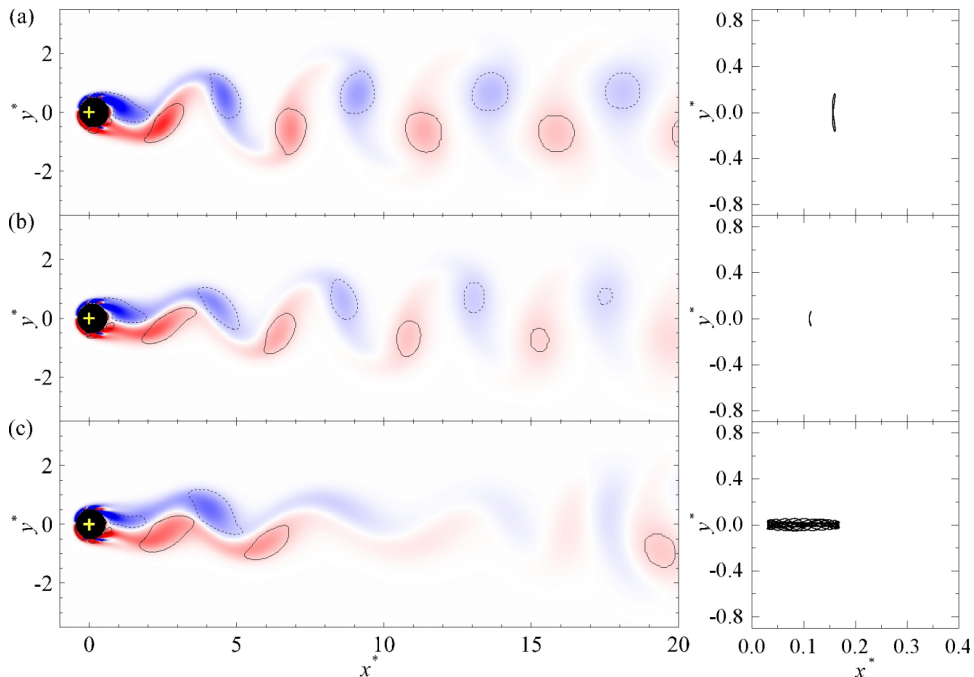

FIG. 7. Wake pattern and cylinder trajectory of the P control cases with (a) $K_p = 6$; (b) $K_p = 12$; (c) $K_p = 18$. Refer to Figure 3 for the colorbar.
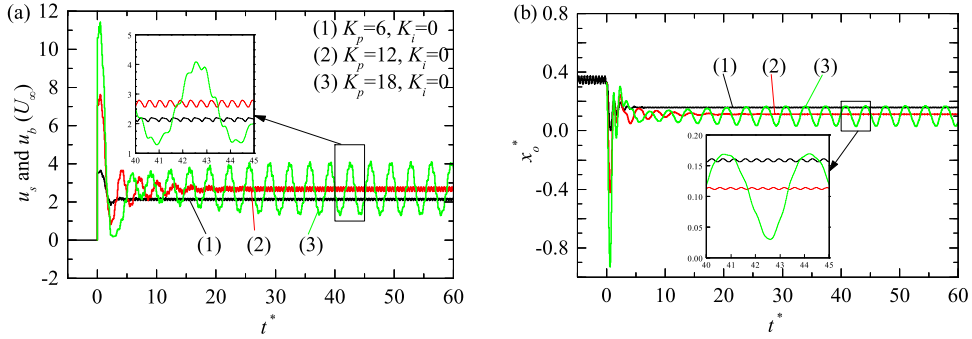
FIG. 8. Time histories of (a) the WSLB velocities (u_s and u_b) and (b) the cylinder's streamwise location (x_o^*) in the three P control cases.

in Figure 7(c), in this case the trajectory of the cylinder becomes disordered and the wake does not converge to a periodical state any more. The cylinder mainly moves back and forth along the streamwise direction.

Time histories of the WSLB velocities (u_s and u_b) and the cylinder's steamwise locations (x_o^*) in the above three cases are compared in Figure 8. As revealed in Figure 8(a), overshoots of u_s and u_b appear in all the three cases after actuating the WSLB at $t^* = 0$, where $t^* = t/T_n$. Since the feedback signals σ_v in these three cases at $t^* = 0$ are identical, it is not surprising to see that the overshoot amplitude increases as K_p increases. As time advances, the overshoot and its subsequent large-amplitude oscillations in the $K_p = 6$ case disappear quickly, and then the velocities and streamwise location reach their respective steady state, i.e., oscillations with small amplitudes. In the $K_p = 12$ case, the subsequent large-amplitude oscillations after the overshoot continue for several more periods and are then gradually replaced by the steady-state small-amplitude oscillations. Unlike in the previous two cases, however, in the $K_p = 18$ case, the large-amplitude oscillations after the overshoot never disappear. The oscillation amplitude decreases first and then increases to reach its steady-state level. Interestingly, it is found that at the steady state, the velocity oscillation and the streamwise location oscillation are out-of-phase, as indicated in the two close-ups in Figure 8. This out-of-phase relation clearly indicates that the motion of the cylinder in this case is excited and dominated by the WSLB.

The current results also help justify the suitability of choosing the standard deviation of the y velocity σ_v as the feedback signal. In the $K_p = 18$ case, if, instead of σ_v, the standard deviation of the x velocity or of the total velocity is used as the feedback signal, very large signal values will be produced by the cylinder's violent streamwise oscillation as shown in Figure 7(c). According to the P control algorithm, these large signal values will result in the increase of the WSLB velocities like what appear in Figure 8(a), which will then induce even more violent streamwise oscillations for the cylinder. Hence, instead of being suppressed, the cylinder's VIV will be amplified.

2. I control

In the I control, four selected cases are investigated, where the integral gain constant K_i varies from 2×10^{-5} to 8×10^{-5} with an interval 2×10^{-5}. It is found that the VIV can be fully suppressed in all these four cases, and the steady-state wakes and cylinder trajectories are similar to those in the open-loop control case with $u_s = u_b = 3.1U_\infty$, as shown in Figure 5(g). This is expected because, according to Equation (10), the WSLB velocities u_s and u_b will keep increasing until the feedback signal σ_v (non-negative) reaches zero, no matter what K_i value (must be positive) is chosen.

Figure 9 compares the time histories of x_o^* and y_o^*, i.e., the cylinder's streamwise and cross-flow displacements. It can be seen that after the WSLB is actuated at $t^* = 0$, the cylinder's streamwise and cross-flow displacements in all the four cases gradually reach constant values and their vibration amplitudes become zero, indicating the complete suppression of the VIV. Similar trends are also found for the WSLB velocities in Figure 10, where u_s and u_b in all the cases increase from zero
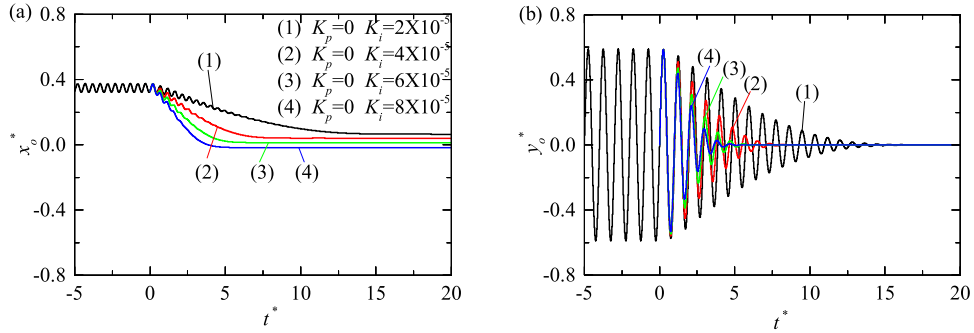
FIG. 9. Time histories of x_o^* and y_o^*, the cylinder's streamwise and cross-flow locations, in the four I control cases.

to their respective final values. As K_i increases, the time required for both the cylinder displacements and the WSLB velocities to reach their respective constant values becomes less, indicating that larger K_i is more efficient in suppressing the VIV. However, it is also found from Figure 10 that the final WSLB velocities increase with the increase of K_i, meaning that larger K_i results in more energy consumption in the steady-state control.

3. PI control

In the PI control, both the proportional gain constant K_p and the integral gain constant K_i in Equation (10) are non-zero. K_p is fixed at 12 at which good VIV control can be achieved in the P control as shown in Figure 6, whereas K_i are set as the same four values in the I control. The simulation results reveal that the VIV can be completely suppressed in all these four cases, and the final status of the cylinder and its wake are also similar to those in the I control cases. However, compared to in the I control cases, the differences in x_o^* and y_o^* among the present four cases are much smaller during both their transient and steady processes, as shown in Figure 11. This is caused by the very similar actuation velocities of these cases as shown in Figure 12(a). In addition, these actuation velocities in the transient process fluctuate with much larger magnitudes than in the I control cases. As a result, amplified fluctuations in x_o^* are observed right after actuating the WSLB, which are then quickly damped within five vortex shedding periods, and fluctuations in y_o^* are damped much faster than in the I control cases.

Time histories of the WSLB velocities in three selected cases are compared in Figure 12(b): one case uses the P control ($K_p = 12$, $K_i = 0$), one uses the I control ($K_p = 0$, $K_i = 2 \times 10^{-5}$), and one uses the PI control ($K_p = 12$, $K_i = 2 \times 10^{-5}$). It can be seen that the velocity history in the PI control case is a hybrid of those in the other two cases. The PI control taps the strength of both the P control and the I control. On one hand, the involvement of P control makes the WSLB velocities very responsive, so that the x_o^* and y_o^* fluctuations and hence the VIV can be suppressed faster
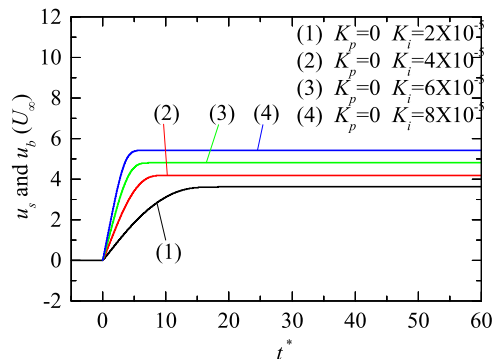

FIG. 10. Time histories of the WSLB velocities in the four I control cases.
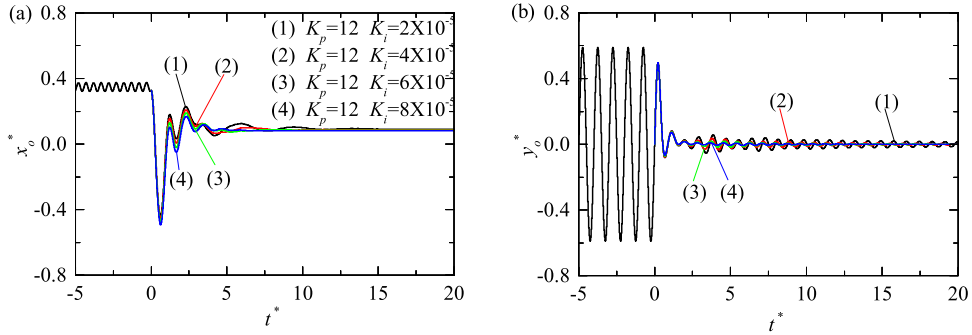
FIG. 11. Time histories of x_o^* and y_o^*, the cylinder's streamwise and cross-flow locations, in the four PI control cases.

than in the pure I control. On the other hand, the involvement of I control makes the complete VIV suppression possible and helps the WSLB velocities achieve their steady state faster than in the pure P control.

To further compare the VIV control performance under different control schemes, a settling time, t_s^*, is defined as the instant when the controlled VIV amplitude starts to fall within 10% of that in the uncontrolled case. Figure 13(a) shows the variations of t_s^* against the integral gain constant K_i in the I and PI control cases. In addition to the trend that the settling time generally decreases with the increase of K_i, it clearly reveals that, at given K_i, the settling time in the PI control is always smaller than that in the I control. This confirms the higher efficiency of the PI control. Moreover, Figure 13(b) reveals that the steady-state WSLB velocities, i.e., u_s^s and u_b^s, in the PI control are smaller than those in the I control, indicating that the energy consumption required for maintaining the control effect is less in the PI control. Therefore, with the above findings and the fact that the P control itself cannot fully suppress the VIV, one can conclude that the PI control outperforms the other two control schemes in terms of both the effectiveness and efficiency.

4. Effect of T_{SD}

In Secs. III C 1–III C 3, the length of data history used for the feedback, T_{SD}, is fixed at T_n, the vortex shedding period in the uncontrolled case, in all the closed-loop control cases. Since the feedback signal σ_v is evaluated over T_{SD}, the transient and steady-state processes of the control depend on the selection of T_{SD}. In this section, hence, the influence of T_{SD} on the VIV control is investigated, with the same PI control parameters as in Sec. III C 3. Seven T_{SD} values are selected, i.e., $T_{SD} = 0$, T_n, $2T_n$, $4T_n$, $6T_n$, $8T_n$, and $10T_n$. Unlike in the other cases where σ_v is evaluated over a period of time, in the $T_{SD} = 0$ case the absolute value of instantaneous y velocity $|v|$ at Point P $(2.67D, 0)$ is used as the feedback signal.
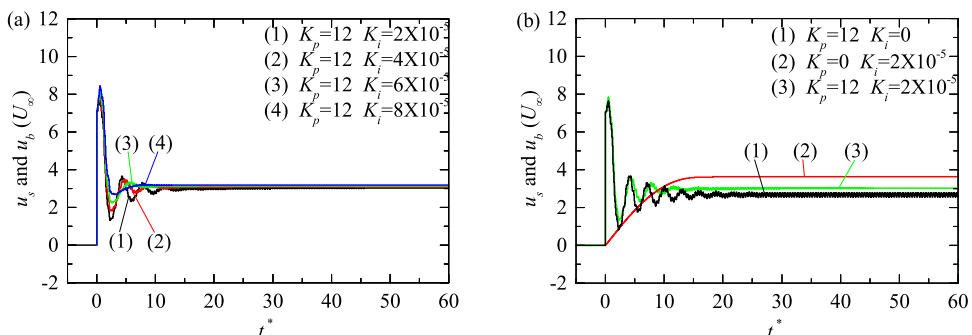

FIG. 12. Time histories of the WSLB velocities in (a) the four PI control cases; (b) three selected cases: one P control ($K_P = 12$, $K_i = 0$), one I control ($K_P = 0$, $K_i = 2 \times 10^{-5}$), and one PI control $K_P = 12$, $K_i = 2 \times 10^{-5}$.
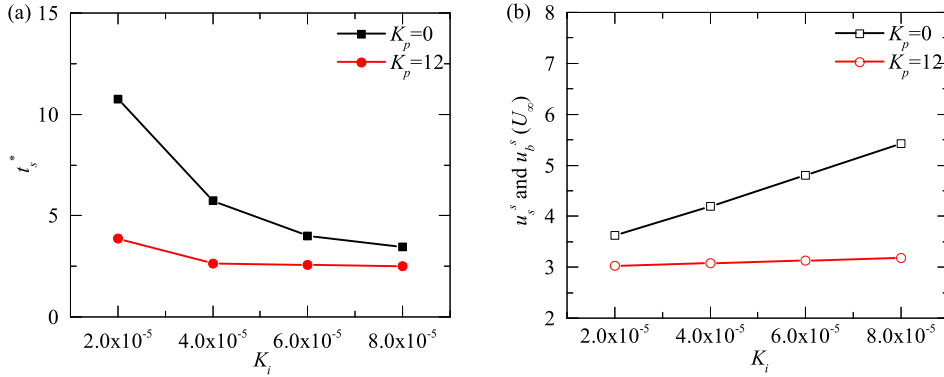
FIG. 13. Variation of (a) the settling time t_s^*; (b) the WSLB velocities against the integral gain constant K_i in the I and PI control cases.

The simulation results confirm that the WSLB is able to fully suppress the VIV with the feedback signal obtained over all the seven T_{SD} values. Figure 14 shows the variations of the settling time t_s^* and the steady-state WSLB velocities against T_{SD}. It can be seen from Figure 14(a) that, with the increase of T_{SD}, t_s^* decreases first and then increases, suggesting the existence of a minimum or optimum t_s^* between $T_{SD} = 0$ and 10. In the present study, the minimum t_s^* appears at either $T_{SD} = T_n$ or $T_{SD} = 2T_n$, depending on the K_i value. As for the steady-state WSLB velocities, it is found from Figure 14(b) that u_s^s and u_b^s do not change too much when T_{SD} is small. However, they increase a lot when T_{SD} increases, especially at large K_i, meaning that larger T_{SD} results in more energy consumption.

The settling time for the open-loop control with the WSLB velocities $u_s = u_b = 3.1U_\infty$ is also plotted in Figure 14(a) for comparison. It is found that the settling time for some of the cases with $T_{SD} = 0$, T_n, and $2T_n$ at large K_i is smaller than that in the open-loop control, with the maximum reduction 41% occurring in the case with $K_p = 12$, $K_i = 6 \times 10^{-5}$, and $T_{SD} = 2T_n$. This indicates that not all the PI controls preform better than the open-loop controls, and selecting suitable control parameters is very important for efficient control. Interestingly, it is also found from Figure 14(b) that the minimum steady-state WSLB velocities required for fully suppressing the VIV in the closed-loop control are near $3.1U_\infty$ that is obtained in the open-loop control. This suggests that, to prevent the cylinder from VIV, the minimum required WSLB velocities are about $3.1U_\infty$, no matter whether the control is open-loop or closed-loop.

5. Effect of sensor location

Since at $Re = 100$ the uncontrolled cylinder wake is intrinsically asymmetric and the standard deviation of the y velocity, σ_v, recorded by the sensor is chosen as the feedback signal in the present
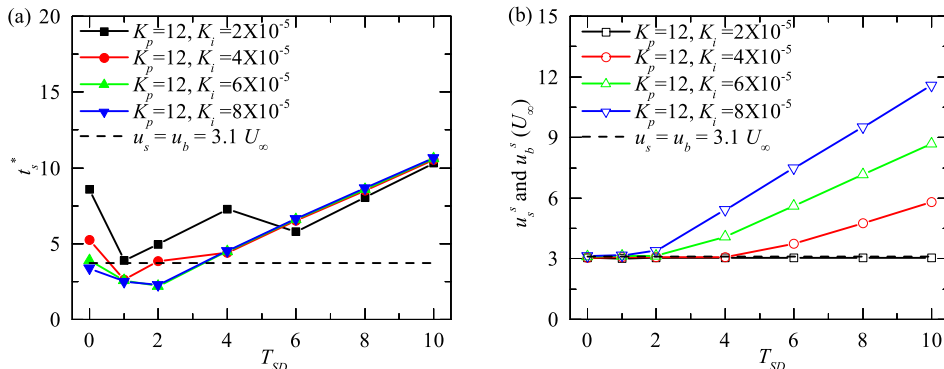

FIG. 14. Variation of (a) the settling time t_s^*; (b) the WSLB velocities against T_{SD}, the length of data history used for the feedback, in the PI control cases.

TABLE II. Selected PI control cases when the sensor is located at Point $(10D, D)$ and at the cylinder center.

PI control cases where the sensor is at	K_p	K_i	u_s^s and u_b^s (U_∞)
Point $(10D, D)$	40	1×10^{-4}	3.1
Point $(10D, D)$	40	1.3×10^{-4}	3.1
Point $(10D, D)$	40	1.5×10^{-4}	3.6
Cylinder center	5×10^{-3}	1×10^{-8}	3.1
Cylinder center	5×10^{-3}	2×10^{-8}	3.1
Cylinder center	5×10^{-3}	4×10^{-8}	3.2

study, it is hypothesized that the VIV control is independent of the sensor location. To confirm this hypothesis, several selected PI control cases listed in Table II are simulated, where the sensor is either placed at a new place in the flow field, i.e., Point $(10D, D)$, or even fixed at the cylinder center. In the latter scenario, instead of σ_v, the standard deviation of the y displacement of the cylinder center, σ_{y_o}, is used as the feedback signal. With the change of sensor location, the corresponding proportional gain constant K_p and integral gain constant K_i are adjusted accordingly to ensure the generation of reasonably large WSLB velocities shortly after the control starts as well as the quick, complete suppression of the VIV. The simulation results reveal that the VIV can be fully suppressed in all these cases. The required steady-state WSLB velocities for the control are also evaluated and listed in Table II. It is found that the required steady-state WSLB velocities are also at least about $3.1U_\infty$, suggesting that the minimum required WSLB velocities do not change with the change of the sensor location.

IV. CONCLUSION

This paper studies the two-dimensional VIV control of a circular cylinder at a Reynolds number of 100 using a novel active control method, i.e., the WSLB actuator that consists of a pair of suction slots on the windward side of the cylinder and a pair of blowing slots on the leeward side. To facilitate this study, an LBM based numerical framework is adopted. Both open-loop and closed-loop controls are considered. In the open-loop VIV control, three types of actuation arrangements, including the pure suction on the windward side, the pure blowing on the leeward side, and the general WSLB on both sides, are implemented and compared. It is found that, among the three, the general WSLB is the most effective in the VIV control, whereas the pure suction is the least effective. In addition, for each type of actuation arrangements, the control effect increases with the increase of actuation velocity.

In the closed-loop VIV control, the basic P, I, and PI control schemes are applied to adjust the WSLB velocities based on the flow information, i.e., the standard deviation of the y velocity σ_v obtained from a sensor. The effects of four key control parameters are investigated, including the proportional gain constant K_p, the integral gain constant K_i, the length of data history used for the feedback T_{SD}, and the location of the sensor. Main findings from this study are as follows:

1. The use of only the P control fails to completely suppress the VIV. But there exists a suitable K_p range in which both the streamwise and cross-flow vibrations are significantly attenuated. In the present study, the best P control occurs at $K_p = 14$.
2. The VIV can be completely suppressed in the I control. Larger K_i is more efficient in the control, but results in more energy consumption.
3. The PI control taps the strength of both the P and I controls: the involvement of P control makes the WSLB velocities very responsive so that the VIV can be suppressed faster, and the involvement of I control makes the complete VIV suppression possible. It is not surprising to see that the PI control outperforms the other two schemes in terms of both the control effectiveness and efficiency.

4. There exists an optimal T_{SD} for the PI control, at which the VIV control is the most efficient. In the present study, this optimal value is close to $T_{SD} = T_n$ and $2T_n$.

5. To fully suppress the cylinder's VIV, there exist the minimum required WSLB velocities, no matter whether the control is open-loop or closed-loop. In the present study, this minimum velocity is about $3.1U_\infty$.

6. The VIV control is independent of the sensor location in the present study.

In the near future, the velocities of the two suction-blowing pairs in the WSLB actuator will be allowed to vary independently, so that the system will be under fully actuated control. In addition, more advanced control schemes, such as the adaptive control method and the fuzzy control method, will be applied to further improve the effectiveness and efficiency of the WSLB enabled two-dimensional VIV control.

ACKNOWLEDGMENTS

[1] H. Choi, W.-P. Jeon, and J. Kim, "Control of flow over a bluff body," Annu. Rev. Fluid Mech. **40**, 113–139 (2008).

[2] M. M. Zdravkovich, "Review and classification of various aerodynamic and hydrodynamic means for suppressing vortex shedding," J. Wind Eng. Ind. Aerodyn. **7**, 145–189 (1981).

[3] H. Oertel, Jr., "Wakes behind blunt bodies," Annu. Rev. Fluid Mech. **22**, 539–562 (1990).

[4] O. M. Griffin and M. S. Hall, "Review-vortex shedding lock-on and flow control in bluff body wakes," J. Fluids Eng. **113**, 526–537 (1991).

[5] W.-L. Chen, D.-L. Gao, W.-Y. Yuan, H. Li, and H. Hu, "Passive jet control of flow around a circular cylinder," Exp. Fluids **56**, 1–15 (2015).

[6] I. Korkischko and J. R. Meneghini, "Suppression of vortex-induced vibration using moving surface boundary-layer control," J. Fluids Struct. **34**, 259–270 (2012).

[7] F. O. Thomas, A. Kozlov, and T. C. Corke, "Plasma actuators for cylinder flow control and noise reduction," AIAA J. **46**, 1921–1931 (2008).

[8] M. Zhang, L. Cheng, and Y. Zhou, "Closed-loop-controlled vortex shedding and vibration of a flexibly supported square cylinder under different schemes," Phys. Fluids **16**, 1439–1448 (2004).

[9] C. Wang, H. Tang, F. Duan, and S. C. M. Yu, "Control of wakes and vortex-induced vibrations of a single circular cylinder using synthetic jets," J. Fluids Struct. **60**, 160–179 (2016).

[10] W.-L. Chen, H. Li, and H. Hu, "An experimental study on a suction flow control method to reduce the unsteadiness of the wind loads acting on a circular cylinder," Exp. Fluids **55**, 1707 (2014).

[11] K. B. Skaugset and C. M. Larsen, "Direct numerical simulation and experimental investigation on suppression of vortex induced vibrations of circular cylinders by radial water jets," Flow, Turbul. Combust. **71**, 35–59 (2003).

[12] L. Du and X. Sun, "Suppression of vortex-induced vibration using the rotary oscillation of a cylinder," Phys. Fluids **27**, 023603 (2015).

[13] F. Xu, W.-L. Chen, Y.-Q. Xiao, H. Li, and J.-P. Ou, "Numerical study on the suppression of the vortex-induced vibration of an elastically mounted cylinder by a traveling wave wall," J. Fluids Struct. **44**, 145–165 (2014).

[14] Z. Chen and N. Aubry, "Closed-loop control of vortex-induced vibration," Commun. Nonlinear Sci. Numer. Simul. **10**, 287–297 (2005).

[15] S. Dong, G. S. Triantafyllou, and G. E. Karniadakis, "Elimination of vortex streets in bluff-body flows," Phys. Rev. Lett. **100**, 204501 (2008).

[16] S. M. Hasheminejad, A. H. Rabiee, M. Jarrahi, and A. Markazi, "Active vortex-induced vibration control of a circular cylinder at low Reynolds numbers using an adaptive fuzzy sliding mode controller," J. Fluids Struct. **50**, 49–65 (2014).

[17] L. Du, X. Jing, and X. Sun, "Modes of vortex formation and transition to three-dimensionality in the wake of a freely vibrating cylinder," J. Fluids Struct. **49**, 554–573 (2014).

[18] S. Poh and A. Baz, "A demonstration of adaptive least-mean-square control of small amplitude vortex-induced vibrations," J. Fluids Struct. **10**, 615–632 (1996).

[19] P. Lallemand and L.-S. Luo, "Theory of the lattice Boltzmann method: Dispersion, dissipation, isotropy, Galilean invariance, and stability," Phys. Rev. E **61**, 6546–6562 (2000).

[20] D. Yu, R. Mei, and W. Shyy, "A multi-block lattice Boltzmann method for viscous fluid flows," Int. J. Numer. Methods Fluids **39**, 99–120 (2002).

[21] P. Lallemand and L.-S. Luo, "Lattice Boltzmann method for moving boundaries," J. Comput. Phys. **184**, 406–421 (2003).

[22] Y. Chen, Q. Cai, Z. Xia, M. Wang, and S. Chen, "Momentum-exchange method in lattice Boltzmann simulations of particle-fluid interactions," Phys. Rev. E **88**, 013303 (2013).

[23] J. Zhou, R. Adrian, S. Balachandar, and T. Kendall, "Mechanisms for generating coherent packets of hairpin vortices in channel flow," J. Fluid Mech. **387**, 353–396 (1999).

[24] S. Izquierdo and N. Fueyo, "Characteristic nonreflecting boundary conditions for open boundaries in lattice Boltzmann methods," Phys. Rev. E **78**, 046707 (2008).

[25] C. H. K. Williamson and A. Roshko, "Vortex formation in the wake of an oscillating cylinder," J. Fluids Struct. **2**, 355–381 (1988).